ELSEVIER

Polymer 41 (2000) 2379–2390

polymer

Temperature studies of optical birefringence and X-ray diffraction with poly(*p*-xylylene), poly(chloro-*p*-xylylene) and poly(tetrafluoro-*p*-xylylene) CVD thin films

J.J. Senkevich*, S.B. Desu, V. Simkovic

Virginia Tech, Department of Materials Science and Engineering, 213 Holden Hall, Blacksburg, VA 24061-0237, USA

Received 19 December 1997; received in revised form 9 March 1999; accepted 1 June 1999

Abstract

The increased demand for low dielectric constant ($k < 3.0$) chemical vapor deposited polymer thin films to replace SiO_2 ($k = 3.9$–4.3) to reduce *RC*-delay in ultra large scale integration (ULSI) devices has prompted the synthesis of many new polymers. However, the ultimate properties of the polymer thin film are determined by its molecular structure that for polymers is often anisotropic. A basic understanding of the structure–property relations and how they are influenced by the molecular architecture is imperative for the future development of polymer thin films in a large number of applications including those in the electronics industry. The study here utilizes X-ray diffraction and variable angle spectroscopic ellipsometry to characterize the optical birefringence and its change as a function of successive post-deposition anneals with poly(*p*-xylylene), poly(chloro-*p*-xylylene), and poly(tetrafluoro-*p*-xylylene). β-PPXN and VT-4 are shown to have a large negative birefringence after a post-deposition anneal. However, PPXC and PPXD show the opposite behavior, exhibiting a small positive birefringence after anneal. Possible reasons for this difference are given.

Keywords: Birefringence; Poly(*p*-xylylene); Poly(chloro-*p*-xylylene)

1. Introduction

An interest exists to reduce *RC*-delay in ultra large scale integration (ULSI) devices by replacing SiO_2 ($k = 3.9$–4.3) with a polymeric material ($k < 3.0$) [1]. Unlike SiO_2, polymeric thin films are often highly anisotropic which largely impacts their properties. Many new low-*k* reasonably high thermal stability polymer thin films have been recently developed both by solution-based [2–5] and chemical vapor deposition (CVD) techniques [6–8]. Most polymers which exhibit high thermal stability contain a main-chain phenyl constituent, including the parylene polymers studied here, polyimides, poly(ether ether ketone), etc. However, the phenyl group possesses a large anisotropic molecular polarizability ($\Delta\alpha = 5.62$ Å^3) which directly affects the polymer's optical and dielectric properties. The polymer thin film's large optical or dielectric anisotropy is only able to be manifested when there is preferential alignment of the polymer chains. Preferential alignment is most apt to take place during polymer crystallization where a higher degree of crystallization may yield more aligned polymer chains and thus a more highly anisotropic thin film [9–20].

The aim of this study is to understand the optical anisotropy in thermal CVD poly(*p*-xylylene) (PPXN), poly(chloro-*p*-xylylene) (PPXC), and poly(tetrafluoro-*p*-xylylene) (VT-4) thin films (Fig. 1) as a function of successive post-deposition thermal anneals. PPXN, PPXC, and VT-4 are from the same class of polymers, namely the parylene polymers. However, the study is general in that the findings and methods presented here using variable angle spectroscopic ellipsometry and X-ray diffraction could possibly be applied to most polymer thin films containing a main-chain phenyl group. In order to integrate low-*k* polymeric materials into ULSI devices their molecular structure by way of their optical anisotropy should be understood and how it changes as a function of successive post-deposition anneals.

2. Experimental

PPXN, PPXC, and VT-4 were deposited using a custom-built CVD reactor with separate sublimation, pyrolysis, and near-room temperature deposition chambers. DPXN,

* Corresponding author. ACT-Microdevices, 7586 Old Peppers Ferry Loop, Radford, VA 24141, USA.

E-mail address: jsenkevich@actmicrodevices.com (J.J. Senkevich)

0032-3861/00/$ - see front matter
PII: S0032-3861(99)00419-X

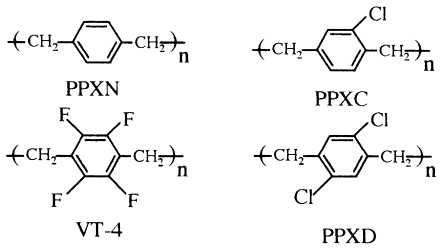

Fig. 1. Repeat units of the parylene polymers studied here.

DPXC, and DVT-4 (the cyclophane precursors) were sublimed at 135, 119, and 95°C to achieve deposition rates of 4.8, 30, and 9 nm/min (estimated) at the substrate temperatures of 28, 28, and 12°C. The PPXN and PPXC films used for optical birefringence versus thickness studies were deposited at various substrate temperatures, sublimation rates, thus producing different deposition rates. All the films were deposited at a base pressure of 0.1–0.12 Torr. The deposition rates depend largely on the substrate temperature and to a lesser extent on the surface conditions of the substrate. The pyrolysis chamber, which converted the cyclophane precursor to the monomer diradical reactive intermediate was heated 600–650°C. The temperature of the substrate was controlled by circulating a ethylene glycol/water solution through copper tubing which surrounded the deposition chamber to obtain temperatures between −6°C to 90°C. The temperature of each individual experiment was controlled accurately by a thermocouple inside the deposition chamber which sat just above the substrate indicating the temperature of the deposition, which could be monitored in situ.

The substrates used for depositing the PPXC films were (111) silicon for both optical and XRD characterization. The silicon wafers were used as received and cut by a carbide scribe into dimensions roughly $1.5 \times 2\ \mathrm{cm}^2$. The thickness and optical characterization was carried out by using a variable angle spectroscopic ellipsometer (VASE) from J.A. Woollam Company, Lincoln, Nebraska. The wavelength of light used was 400–1000 nm and three angles normal to the sample were used: 60, 70, and 75°. The parameters obtained from VASE were delta and psi which are trigonometric parameters that characterize the resultant ellipsoid after linearly polarized light is polarized ellipsometrically after interacting with the thin film. An anisotropic Cauchy model was fitted to delta and psi generating a thickness value and dispersion curves for the out-of-plane and in-plane indices of refraction for each polymer thin film. X-ray diffraction data was obtained using a Scintag XDS-2000 (Sunnyvale, CA, USA) X-ray diffractometer with Cu Kα radiation of 1.5418 Å. Scans were made from 10 to 25° (2θ) for the polymer thin films deposited onto (111) Si in reflection mode.

3. Optical birefringence background and X-ray pole figure analysis

3.1. Theoretical

Poly(*p*-xylylene), poly(chloro-*p*-xylylene), and poly-(tetrafluoro-*p*-xylylene) deposited for this study all contain main-chain phenyl groups. A phenyl group in the main-chain (as opposed to a side group as in polystyrene) enables the polymer to possess a higher thermal stability due to the aromatic's higher bond strength and due to its ability to stabilize adjacent bonds. Benzene is a planar molecule with delocalized π-bonding and exhibits strong anisotropic molecular polarizability. Much work has been focused on understanding the optical polarizability of benzene. In the plane of the benzene molecule, the molecular polarizability is 12.27 $\mathrm{Å}^3$ and perpendicular to the plane it is 6.65 $\mathrm{Å}^3$. The anisotropic molecular polarizability of benzene is then $\Delta\alpha = 5.62\ \mathrm{Å}^3$ [21]. This anisotropy, which is evident in the repeating unit of the polymer, is also manifested in the optical birefringence of the polymer thin films. The birefringence is related to the difference in molecular polarizabilities by differentiating the Lorentz–Lorentz equation, which assumes a spherically symmetric internal field [22].

$$\frac{n^2 - 1}{n^2 + 2} = \frac{4}{3}\pi P \tag{1}$$

where n is the index of refraction and P is the polarization per unit volume of the material. Differentiating this equation gives:

$$\Delta n = \frac{2}{9}\frac{\pi(n^2 + 2)^2}{n}\Delta P \tag{2}$$

where $\Delta n = n_{\text{out-of-plane}} - n_{\text{in-plane}}$ is the birefringence, and n is the average index of refraction given in terms of the laboratory set-up here:

$$n = \frac{n_{\text{out-of-plane}} + 2n_{\text{in-plane}}}{3} \tag{3}$$

where $n_{\text{out-of-plane}}$ is the index of refraction normal to the substrate and $n_{\text{in-plane}}$ is the index of refraction in the plane of the thin film for an uniaxially oriented polymer. Eq. (2) can be further developed by noting that the polarization difference ΔP is composed of the summation of the different anisotropic molecular polarizabilities of a bond, molecule or segment $(b_i - b_2)$, N_S is the number of segments per unit volume and an orientation factor (f_{Hi}) sometimes called Hermann's orientation function.

$$\Delta P = \sum_{i=1}^{n} N_{Si}(b_i - b_2)_i f_{Hi}, \tag{4}$$

$$f_H = \sum_{i=1}^{n} \frac{3\langle\cos^2\phi_{li}\rangle - 1}{2}, \tag{5}$$

where f_H is given by the second moment of the orientation

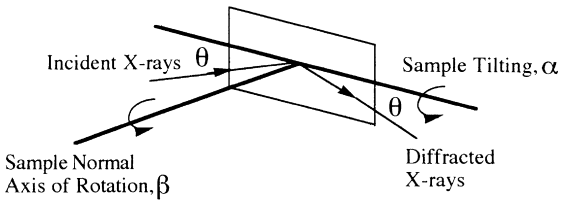

Fig. 2. X-ray pole figure coordinate system.

distribution function and ϕ_{li} is the angle between the *n*th bond, molecule or segment and a reference axis *l* in the case here a vector lying in the plane of the film. The second moment of the orientation distribution function can be found by linear dichroism in the infrared [23–25], polarized Raman scattering [26], microwave methods [27,28], and X-ray pole figure analysis [29–31].

To arrive at Hermann's orientation function by way of X-ray pole figure analysis a diffraction peak must be obtained by a θ–θ or a θ–2θ scan depending on the X-ray diffractometer geometry. In the present study, this was accomplished as a function of increasing post-deposition anneal temperature. Then choosing a diffraction peak (if more than one is available), and which is normally the dominant peak, two operations are performed according to Fig. 2. The sample is tilted from 0 to 90° (α) and at periodic intervals, e.g. 5 or 10° (α), and the sample is rotated 360° (β) at each α. For uniaxial symmetric orientation such as in the present case no rotation is necessary but only tilting from 0 to 90° (α). For purposes of calculating Hermann's orientation function the complementary tilting angle ϕ is used instead of α, of course they are related by: $\phi = 90° - \alpha$. The mean-square cosine value is related to the rotation and tilt intensity scans by:

$$\langle \cos^2 \phi_{hkl,z} \rangle = \frac{\int_0^{\pi/2} I(\phi) \sin \phi \cos^2 \phi \, \mathrm{d}\phi}{\int_0^{\pi/2} I(\phi) \sin \phi \, \mathrm{d}\phi} \tag{6}$$

$$I(\phi) = \int_0^{2\pi} I(\phi, \beta) \, \mathrm{d}\beta. \tag{7}$$

First, the intensity distribution needs to be integrated over the rotation angle β from 0 to 2π then integrated over the complementary tilt angle ϕ from 0 to $\pi/2$. Following the method (outlined by Alexander [32], originally developed by Stein [33] for polyethylene which is orthorhombic and latter generalized by Wilchinsky [31,34] for non-orthorhombic crystal systems) to relate the mean-square cosine value of an analyzed diffraction peak $\langle \cos^2 \phi_{hkl,z} \rangle$ to the *c* crystallographic axis of the hexagonal unit cell of β-PPXN to fiber axis (*Z*, parallel to the substrate) of the sample, the following relation may be derived:

$$\langle \cos^2 \phi_{c,z} \rangle = 1 - 2\langle \cos^2 \phi_{040,z} \rangle. \tag{8}$$

This is valid for the (040) diffraction plane for the hexagonal unit cell of β-PPXN. Only one independent (*hkl*) plane is needed for the hexagonal crystal system independent of the plane, e.g. (*hkl*), (*hk*0), (*h*0*l*), or (00*l*). Unfortunately, a minimum of two independent (*hk*0) planes are needed for the monoclinic crystal system and possibly three if (*h*0*l*) planes are used [30]. For α-PPXN and PPXC, both monoclinic, only one reflection exists therefore the orientation of the *c* crystallographic axis to the fiber axis *Z* is inaccessible.

So far it has been assumed that the measured optical birefringence is solely due to the crystal nature of the polymer thin film. However, the birefringence can be associated with other factors given by the following relation:

$$\Delta = \Delta_c + \Delta_{amorph} + \Delta_{distort} + \Delta_{form} \tag{9}$$

where Δ_c is due to crystal orientation, Δ_{amorph} is due to amorphous orientation, $\Delta_{distort}$ is due to distortional effects primarily associated with a stress unbalance in the polymer thin film, and Δ_{form} is the form birefringence related to multiphase structures where domains exist possessing different indices of refraction. Further for form birefringence, the domains need to be non-spherical or preferentially arranged and the spacings between the two domains $\lambda_m/20$, where λ_m is the wavelength of light in the medium [35]. For the PPXN thin films this would mean spacing from 33 to 83 nm for light of wavelength of 400–1000 nm and an index of refraction for PPXN (as-deposited) of 1.66. This last criterion might not apply for PPXN or the other homopolymer parylenes. For purposes of an "order of magnitude" calculation the following relation may be used.

$$n_{\parallel} - n_{\perp} = \frac{\phi_1 \phi_2 (n_1^2 - n_2^2)^2}{2n_a[(\phi_1 + 1)n_2^2 + \phi_2 n_1^2]}, \tag{10}$$

$$n_a = \phi_2 n_2^2 + \phi_1 n_1^2. \tag{11}$$

Using the values of 1.650 for the as-deposited PPXN polymer (for the amorphous phase) and 1.686 after a 350°C anneal (for the crystalline phase) as a rough starting point and a percent crystallinity of 82% a value of 0.000069 for $n_{\parallel} - n_{\perp}$ was found. If it is assumed that 50% crystallinity exists then $n_{\parallel} - n_{\perp}$ increases to 0.000235. With either calculation the contribution of form birefringence to the total birefringence is negligible. These calculations correspond well to what was previously known about form birefringence's contribution to the overall birefringence in most semi-crystalline polymers [35].

At higher degrees of crystallinity between the T_g and T_m the crystalline phase of the polymer cannot easily stress relax and therefore two consequences may result. First, the high degree of crystallinity will have an effect on the orientation of the amorphous phase, i.e. it can no longer be considered random. Second, both the rigid amorphous and the crystalline phases cannot easily stress relax and therefore it should be expected that an increase in film stress should occur as the film is annealed at higher temperatures approaching its T_m. The stress is primarily due to the

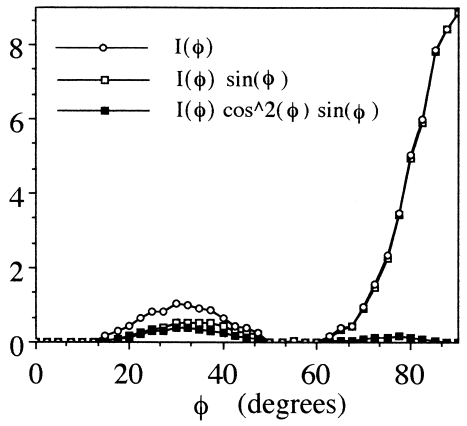

Fig. 3. X-ray pole figure intensity and weighted functions versus complementary tilt angle ϕ.

coefficient of thermal expansion mismatch between the polymer thin film (35–69 ppm/°C) and the silicon substrate (3.35 ppm/°C) directly proportional in Eq. (12) [36]:

$$\sigma_{\text{thermal}} = \frac{-E\Delta\alpha(T_2 - T_1)}{1 - \nu} \tag{12}$$

where σ_{thermal} is the thermal stress, E is the modulus of elasticity, $\Delta\alpha$ is the difference in the coefficient of thermal expansion between the film and substrate, T_2 is the anneal temperature, T_1 is the deposited temperature, and ν is Poisson's ratio of the film. The increase of film stress with an increase in anneal temperature has shown to be valid previously [37]. The modulus of elasticity for PPXN is 2.4 GPa, CTE = 69 ppm/°C, and $\nu \sim 1/3$. For a anneal temperature of 250°C this gives a predicted stress of 53 MPa. This assumes that PPXN was deposited at 25°C, no stress relaxation took place, and the as-deposited polymer did not possess any intrinsic stresses. Experimentally, PPXN had an as-deposited compressive stress of −18 MPa. The film reached a peak tensile stress of 53 MPa at 270°C at which point the phase change from α to β fully occurred and the stress subsequently dropped to 33 MPa. Experimentally, these samples were heated to the anneal temperature and then effectively quenched not allowing any molecular rearrangements upon cooling to reach an equilibrium state. The stress again increased at higher anneal temperatures. PPXC like PPXN showed a compressive stress as-deposited. With higher anneal temperatures the stress increased until reaching a maximum value of 33 MPa at 250°C just before its melting point.

3.2. Experimental

An important consideration when studying the birefringence of polymer thin films is to have some idea of their orientation. Orientation may be greatly influenced by polymer crystallization by either a stress-induced mechanism or simply by thermal anneals [9–15,38,39]. However, as previously eluded to, the polymer's birefringence is composed of not simply the crystalline fraction but possibly the amorphous fraction, distortional effects, and form effects. A previous study by You et al. [40] investigated the texture of PPXN as-deposited at room temperature, annealed at 200°C for 30 min., annealed at 300°C for 2.5 h, and annealed at 350°C for 12 h. The sample annealed at 350°C possessing the hexagonal β-phase will be analyzed here to determine its orientation. Then a comparison can be made between this analysis and the thermal studies undertaken here.

Fig. 3 shows the intensity distribution function as a function of the complementary tilt angle in degrees. Additionally, the weighted functions are plotted in accordance with Eqs. (6) and (7). You et al.'s study indicated that PPXN exhibited axial sample symmetry, e.g. the same intensity variation with sample rotation β as a function of tilt angle α. As a result Eq. (7) can be ignored making the calculations more simplified. Integrating the area under the, $\{I(\phi)\sin\phi\cos^2\phi\}$ versus $\phi($ curve and likewise with $\{I(\phi)\sin\phi\}$ versus ϕ and then using Eq. (6) yields a value of 0.0846 for $\langle\cos^2\phi_{040,z}\rangle$. However, a more useful quantity is $\langle\cos^2\phi_{c,z}\rangle$ the mean-square cosine value of the c crystallographic axis of the hexagonal unit cell of β-PPXN to the fiber axis Z (parallel to the substrate). Using Eq. (8) yields a value of 0.831. Finally, the Hermann's orientation function can be calculated by use of Eq. (5) yielding a value of 0.746. This can be compared to a perfectly oriented sample $f_H = 1$ where the diffraction planes are parallel to the substrate, to random orientation $f_H = 0$, and to $f_H = -0.5$ where the diffraction planes are perpendicular to the substrate. Evidently a high degree of order exists in β-PPXN post-deposition annealed at elevated temperatures.

Eqs. (2) and (4) yield:

$$\Delta n = \frac{2}{9}\frac{\pi(n^2+2)^2}{n}\sum_{i=1}^{n} N_{Si}(b_i - b_2)_i f_{Hi}. \tag{13}$$

Here it will be assumed that each crystallizable segment has the same orientation (e.g. phenyl group, methylene group, etc.) since X-ray pole figure analysis only gives an average value. To determine the orientation of individual molecules linear dichroism is needed. The following values are needed to calculate the birefringence based on the orientation data from above: average index of refraction at 350°C determined from this study 1.686, the number of segments per unit volume 0.00667 Å^3 (16 segments in a monoclinic unit cell of dimensions of $a = 20.52, c = 6.58$) [41] and the segmental anisotropic molecular polarizability. The segmental anisotropic molecular polarizability deserves special attention since it is the largest source of error for the calculations of the crystalline birefringence. In the most simplest sense the PPXN repeat unit may be viewed as a phenyl group in series with two methylene groups in which case the anisotropic molecular polarizability would be 5.62 and 0.721 Å^3 from Dewar et al. [21] and Stein [42]. The later value of 0.721 Å^3 is derived from studies of

Table 1
Contibutions to measured birefringence of PPXN ($X_c = 0.6$, $\Delta n_{tot} = -0.1304$, film thickness = 175 nm)

	Δn_{amorph}	Δn_c
$(b_i - b_2)_{isolated\ seg.}$ (-6.34 Å^3) Dewar et al.	0.133	− 0.306
Δn_{tot} (corrected) −0.209	−0.0635	− 0.306

polyethylene and the anisotropic molecular polarizability of its repeat unit. Adding both values together yields 6.34 Å^3 for the addition of both segments [43].

Two fundamental sources of uncertainty exist with respect to the calculation of PPXN's crystalline birefringence. The segmental anisotropic molecular polarizability of PPXN's repeat unit is not well known. Further, the Lorentz–Lorentz equation assumes a spherically symmetric internal field which is often a poor assumption for a segmental unit not isolated but residing in an ordered condensed phase state. To add to the uncertainty, the internal field effect often may produce an experimental segmental anisotropic molecular polarizabilities 100% higher than the gas-phase anisotropic molecular polarizability of the analogous isolated molecule [38,39,42]. The second source of uncertainty has to do with the orientation of the PPXN chain as it approaches the silicon substrate/thin film interface. A previous study has shown as annealed films become thinner their birefringence becomes more positive and below ~90 nm it rapidly increases to 0.05–0.08 from −0.11 [44]. There is no reason to believe this thickness regime (0–50 nm) becomes more oriented just because the film is thicker. Therefore, the true film birefringence of PPXN should be measured for a film which does not feel the effects of the substrate. Such a film would be a free-standing film and no longer a thin film. If a 50 nm film has a 0.065 birefringence after a 325°C anneal then the 175 nm film with a birefringence of −0.1304 has a corrected birefringence of −0.209. This corrected value gives a more reasonable value −0.0635 for the amorphous phase of PPXN. What should be apparent here is that too many uncertainties exist to quantitatively relate a change in birefringence with an increase in the degree of crystallinity in the films. This is not to say that an increase in the degree of crystallinity is not responsible for a more negative birefringence of PPXN. However, chain orientation is not homogenous throughout the film but varies from the silicon substrate outward.

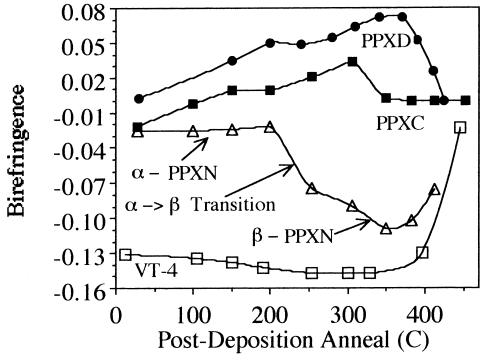

Fig. 4. Birefringence versus 30 min successive post-deposition anneals in nitrogen.

The orientation of PPXN's amorphous phase is not necessarily zero. PPXN possesses a broad T_g centered at ~13°C the consequences of which imply the amorphous phase has some degree of chain mobility [45]. Flexible chain polymers in the amorphous state with low degrees of crystallinity should be optically isotropic. This is in contrast to rigid-rod amorphous polyimide thin films which often exhibit considerable birefringence as high as $\Delta n = -0.222$. [46] However, most polyimides normally exhibit a high T_g preventing much polymer chain mobility at room temperature. What was once isotropic for the amorphous phase of PPXN can become much more anisotropic and thus birefringent when the thin film reaches higher degrees of crystallinity. Mostly since the amorphous phase can become ordered due to near-neighbor highly ordered crystalline regions. It would not be surprising to find that the amorphous phase of PPXN at a degree of crystallinity of 0.80 would be highly ordered and thus contributes to the overall measured birefringence. Also, films of less than 80 nm exhibit positive birefringence in contrast to thicker films. Those ultra thin films apparently are influenced by the presence of the substrate.

The experimentally measured birefringence of β-PPXN was −0.1090 and −0.1304 at film thicknesses of 93 and 175 nm obtained at 350°C and 280°C. Clearly, the film thickness affects the birefringence as seen previously [44]. Using Eq. (13) to calculate a crystalline birefringence (from the 175 nm film), and then Eq. (14) (ignoring stress effects) the following values are obtained for the crystalline and amorphous birefringences as seen in Table 1.

$$\Delta n_{amorph} = \frac{\Delta n_{tot} - X_{cv}\Delta n_c}{1 - X_{cv}}. \quad (14)$$

More studies need to be undertaken to understand the effect stress and the amorphous phase has on the film's overall experimentally determined birefringence. Swelling experiments carefully conducted should be able to determine the amorphous phase contribution. Stress, since it is intrinsic is much more difficult to measure and relate to the birefringence in a thin film; that is independent of varying the degree of crystallinity.

3.2.1. Poly(chloro-p-xylylene)

The birefringence of the polymer thin films studied here is a strong function of the polymer's post deposition anneal temperature as seen in Fig. 4. Much information is contained here since optical birefringence is sensitive to the degree of crystallinity, crystal phase transformations, melting phenomena, and to degradation as will be explained. PPXC as shown in Fig. 4 exhibits a positive increase in its birefringence as the polymer is successively

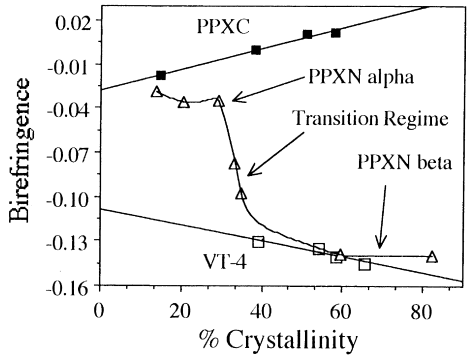

Fig. 5. Birefringence versus percent crystallinity from XRD data.

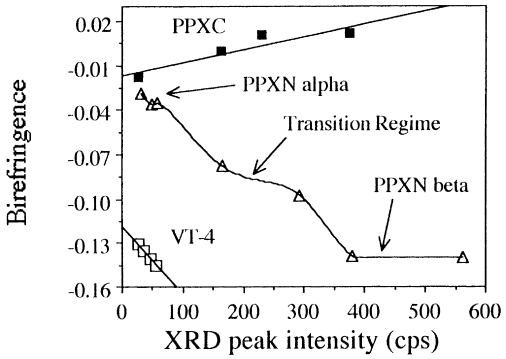

Fig. 7. Birefringence versus XRD peak intensity taken from the most intense diffraction plane in each spectra.

annealed at higher temperatures up to its melting point at 290°C. The increase in birefringence may be attributable to an increase in the degree of crystallinity as measured by X-ray diffraction. An apparent linear increase in birefringence for PPXC with percent crystallinity was found as shown in Fig. 5. The percent crystallinity was found by measuring the relative amorphous and crystalline regions of each XRD spectra in raw data format. Relatively large errors result from this method (±5%) due to uncertainties in determining the area of the amorphous phase. Also, a completely amorphous or completely crystalline parylene thin film is difficult to achieve since nearly all the parylene polymers are semi-crystalline as-deposited and never reach an equilibrium amorphous melted state. The later observation is caused by polymer degradation or in the case of PPXC and PPXD (which possesses two chlorine atoms per phenyl group) the melt transition disrupts the film structure irreversibly. Due to large uncertainties in the percent crystallinity values, the intensity values for the (020) diffraction plane of the monoclinic unit cell for PPXC, as shown in Fig. 6, was taken and plotted versus the birefringence (Fig. 7). An apparent linear relation also exists in Fig. 5. Therefore, most likely the increase in birefringence for PPXC is caused by an increase in crystallinity.

Most of the studies correlating birefringence with degree of crystallization have done so with stretched rubber. It most of these studies crystallization has been something to be avoided [10,11,13,14,16]. There is little doubt that an increase in the degree of crystallinity leads to an increase in the birefringence of the polymer. However, the largest uncertainty resides in the origin of the measured birefringence. Since the overall birefringence is composed of: crystalline, amorphous, distortional, and form effects, factors such as the intrinsic stress of the film could largely impact the measured birefringence. Stein [42] has suggested that the stress and birefringence be simultaneously measured to satisfy this uncertainty. Experimentally, this has been undertaken with bulk polymers [20,47], however, a different experimental approach would need to exist for thin film polymers. Further, nearly all the experiments with birefringence involve stretching the polymer which generates birefringence versus extension ratio and associated plots.

Of particular interest to the study here is PPXC's increasing birefringence with an increase in anneal temperature. The major difference between PPXC and PPXN is the presence of chlorine which increases the anisotropic molecular polarizability of chlorobenzene $\Delta\alpha = 7.00$ [3] versus benzene $\Delta\alpha = 5.62$[3]. Then, with the same orientation and stress PPXC would exhibit a greater birefringence versus PPXN. The increasing birefringence of PPXC probably indicates the plane of the benzene ring is aligning more perpendicular to the substrate, since $n_{\text{out-of-plane}} > n_{\text{in-plane}}$.

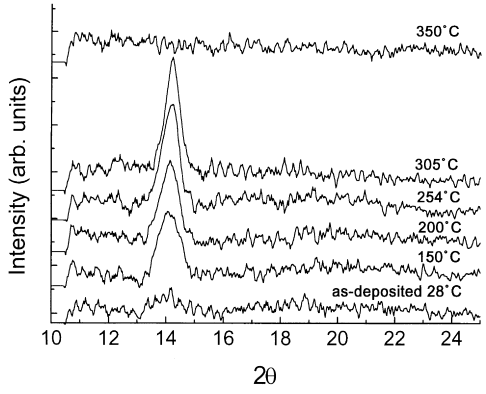

Fig. 6. XRD spectra of PPXC. Peak present is from the (020) diffraction plane of the monoclinic unit cell.

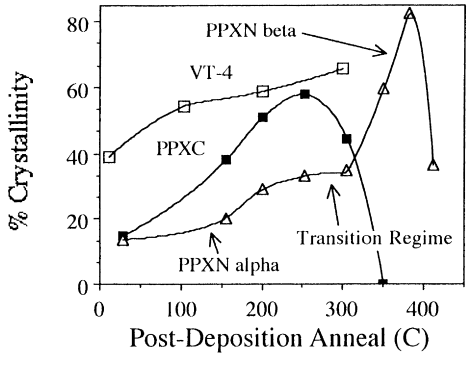

Fig. 8. Percent crystallinity versus 30 min successive post-deposition anneals in nitrogen taken from XRD data.

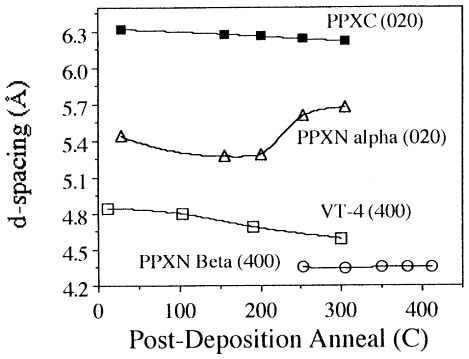

Fig. 9. *d*-Spacings from the XRD data versus 30 min successive post-deposition anneals.

As can be seen from Fig. 8, the crystallinity reaches a peak at ~250°C but the birefringence does not reach a peak until ~300°C, after which point a decline in the birefringence exists and PPXC becomes amorphous as seen by XRD. This abrupt change in the birefringence and crystallinity of PPXC is due to the presence of the melting point at ~290°C. The melt transition causes large permanent morphological changes due to the constrainment imposed by the dimensions of the thin film and the rotation of the phenyl group of PPXC [48]. This rotation disrupts the crystallites and the conformation of the phenyl group's nearest neighbors. The discrepancy between the birefringence and the percent crystallinity peaks is likely attributable to small crystallites of lower melting point becoming a highly oriented amorphous phase. Larger crystallites with smaller *d*-spacings yielding a smaller full width half max (FWHM) have a lower surface free energy, which effectively increases their enthalpy of melting. J.J. Thompson originally derived the formula to relate the decrease in melting temperature for crystals of non-infinite size [49].

$$T_m = T_{m^0}\left[1 - \frac{6\sigma}{a\Delta H_0}\frac{M}{\zeta}\right] \tag{15}$$

where T_m is the melting temperature for the non-infinite crystal, T_{m^0} is the ideal melting point for the infinite crystal, a is the edge length for a cubic crystal, ΔH_0 is the enthalpy of melting, M is the molecular weight of the polymer, ς is the density of the crystal phase, and σ is the surface energy of the crystal. Typically, a Hoffman–Weeks plot is produced from the observed equilibrium melting temperature versus crystallization temperature, where a linear extrapolation can yield T_{m^0} at the intersection of that line and $T_m = T_c$. [50] This experiment is not possible with CVD polymers since cooling from the melt to crystallize the polymer is often not possible. Further, the large-scale motion associated with a melt transition to reach an equilibrium liquid state is often not possible since the dimensions of the thin film prevent this from occurring. Then, the melt transition is often an irreversible one. The polymer thin film does not become isotropic until just before its degradation temperature (~400°C).

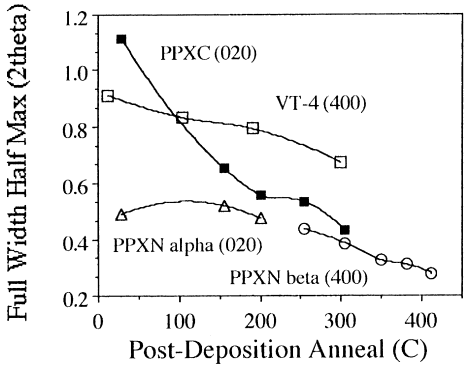

Fig. 10. Full Width Half Max (FWHM) taken from the most intense peak versus 30 min successive post-deposition anneals.

Two further conclusions can be made about PPXC with respect to XRD. Fig. 9 shows the *d*-spacing of PPXC and the other parylene polymers as a function of successive post-deposition anneals. As can be seen, PPXC exhibits a decrease in *d*-spacing as it is annealed at higher temperatures. This is not uncommon since many polymers show paracrystalline behavior, meaning the crystalline phase is slightly disordered yet shows periodicity [51]. Paracrystallinity is apparent with most polymers and reasonable for CVD polymers since they often polymerize crystallize simultaneously. This occurs for PPXC even below its glass transition temperature (~36°C). Under these conditions the localized heating due to polymerization initially and then the heat due to crystallization later promotes crystallization even though the substrate temperature is below T_g. This phenomenon is only possible at higher sublimation rates which may promote higher localized heating. Crystallization during polymerization has been well covered by Wunderlich and colleagues [52–56].

The full width half max (FWHM) of PPXC versus post-deposition anneal is shown in Fig. 10. PPXC exhibits a precipitous drop in its FWHM from the as-deposited sample to the sample annealed at 150°C. This corresponds well to large increase in the percent crystallinity and a large increase in the peak height of the (020) diffraction plane. A decrease in the FWHM could be possibly due to three factors: a decrease in the stress of the crystallite, an increase in the crystalline perfection, and an increase in crystallite size. The as-deposited PPXC stress was measured as −10 MPa (compressive) and after a 150°C anneal 27 MPa (tensile) and slowly increases as the annealing temperature is increased [37]. Using Eq. (12) with PPXC parameters of: $E = 3.2$ GPa, CTE = 35 ppm/°C, and $\nu = 1/3$ gives 34 MPa for a $\Delta T = 225$°C. Experimentally, the stress was 33 MPa. The silicon substrate has an order of magnitude smaller coefficient (~3 ppm/°C) of thermal expansion than PPXC (~35 ppm/°C). Some degree of stress relaxation in the polymer's amorphous phase can take place above its T_g. Then when cooled, the PPXC film wants to contract faster than the silicon

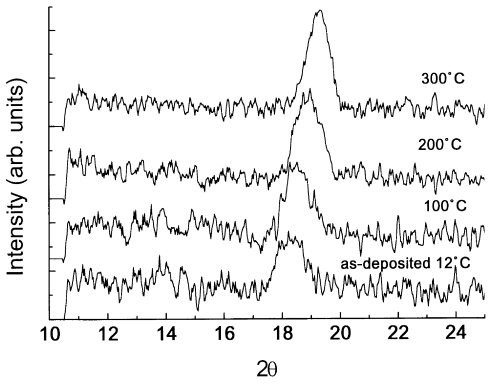

Fig. 11. XRD spectra of VT-4. Peak present is from the (400) diffraction plane of the hexagonal unit cell.

substrate will let it, hence the tensile stress. This situation is similar to nearly all thin film polymers grown on silicon and then annealed.

Two more explanations for the reduction in FWHM is the increase in crystalline perfection and the increase in crystallite size. PPXC's *d*-spacings decrease as a function of post-deposition anneal lending to a decrease in FWHM. However, more significant is the increase in crystallite size as measured by the percent crystallinity, where the percent crystallinity increases considerably from 16% as-deposited to 38% after a 150°C post-deposition anneal (Fig. 8). Likely, the FWHM decreases as the percent crystallinity increases until 290°C. At this point, according to Eq. (15) the smaller crystallites transform into an oriented amorphous phase and the larger crystallites become more perfect (smaller *d*-spacing, smaller FWHM, and more intense (020) diffraction peak).

3.2.2. Poly(tetrafluoro-p-xylylene)

The 282 nm as-deposited VT-4 thin film exhibited a large negative birefringence compared to either the PPXC or PPXN as-deposited thin films. VT-4 apparently possesses a high degree of crystallinity in the as-deposited condition as opposed to PPXN or PPXC, however, many factors may contribute to this difference such as deposition rate as related to sublimation rate of the precursor, substrate temperature, and system pressure. According to its XRD spectra (Fig. 11), VT-4 does not go through any crystal transformations much like PPXC except its *d*-spacings coincide with PPXN to a great extent (in its high temperature $T > 220$°C β-phase). The experimentally determined lattice constants for PPXN are: $a = 20.52$, $b = 20.52$, $c = 6.58$ Å for the hexagonal unit [57]. The study here showed the $a = b = 20.06$–20.10 Å varying slightly at lower annealing temperatures where the $\alpha \rightarrow \beta$ phase transformation was not totally complete. Assuming VT-4 has the same crystal structure as β-PPXN, $a = b = 22.40$–21.09 Å for the (400) diffraction plane. At high temperatures (~380°C) the VT-4 lattice constant is ~5% larger than that of β-PPXN, which is reasonable since fluorine occupies more space than hydrogen thus increasing the lattice constant. They may have the same crystal structures due to the birefringence data, where VT-4 has a similar birefringence to β-PPXN at all temperatures up to its degradation temperature (400°C). More study should be undertaken to confirm this finding. Further evidence for VT-4's crystal structure comes from comparing PPXC to α-PPXN where they are both monoclinic. The *b*-axis lattice constant for PPXC is 12.48 Å (at 250°C) where α-PPXN is 10.58 Å (at 200°C), which is 18% larger. Chlorine is much larger than fluorine therefore this result is not surprisingly. The lattice constant $a(=b)$ of VT-4 should be nevertheless larger than that of β-PPXN due to the presence of fluorine atoms.

As it can be seen from Fig. 4, VT-4 becomes more negatively birefringent up to its degradation temperature (~400°C), where a rapid increase in the birefringence occurs as a result of bond disruption. Birefringence linearly decreases with an increase in crystallinity as seen in Fig. 5. Like PPXC, VT-4 exhibits a decrease in its *d*-spacing with increasing post-deposition anneal temperature (Fig. 7). The drop in *d*-spacing compared to PPXC is much larger which could be related to its high degree of crystallinity as-deposited.

The decrease in FWHM of VT-4 is attributed to the same factors as that of PPXC since they both exhibit similar behavior due to their similar above room temperature T_g's (PPXC ~ 36°C, VT-4 ~ 64°C). The effective slope of the FWHM versus post-deposition anneals (Fig. 10) is smaller compared to PPXC due to a smaller increase in percent crystallinity versus post-deposition anneal. The reduction in the FWHM should be most significant between the as-deposited sample and the annealed samples if stress is the only consideration. However, the largest increase in percent crystallinity is also between the as-deposited sample and the first anneal at 100°C. The main differences between VT-4 and PPXC are: VT-4's crystal structure, as evident from the birefringence data, which influences the orientation of the polymer thin film, the percent crystallinity of VT-4 in the as-deposited condition (~39% for VT-4 and ~16% for PPXC), and the large crystal disorder of VT-4 compared to PPXC. Most significant of the above findings is the phenyl groups in the main-chain of VT-4 are aligned in the plane of the substrate versus PPXC whose phenyl groups tend to align more perpendicular to the plane of the substrate. This finding has large implications for the dielectric constant of VT-4 both in-plane and out-of-plane of the thin film. Namely, the large negative birefringence of VT-4 will cause it to have a large in-plane capacitance and a relative low out-of-plane capacitance not desirable for ULSI devices.

3.2.3. Poly(p-xylylene)

Due to PPXN's crystallographic phase change α (monoclinic) to β (hexagonal) starting at 220°C its measured birefringence is more complicated than either VT-4 or PPXC. Most significant, PPXN has a $T_g = 13$°C which is below room temperature, much different then either PPXC

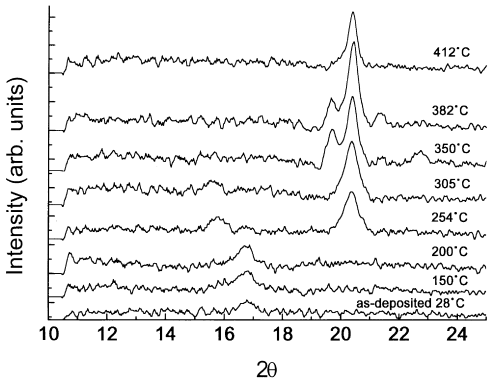

Fig. 12. XRD spectra of PPXN. Peak at low temperatures is present is from the (020) diffraction plane of the monoclinic unit cell and the large peak at higher temperatures is from the (400) diffraction plane of the hexagonal unit cell.

(36°C) or VT-4 (64°C) which have T_g's both above room temperature. The α form of PPXN has the same monoclinic structure of PPXC and it has been previously proposed that VT-4 has the same hexagonal structure of β-PPXN. As can be seen from Fig. 4, the birefringence does not change much up to 200°C but thereafter it rapidly becomes more negatively birefringent due to the formation of β-PPXN.

Fig. 12 shows the XRD spectra of PPXN. the peaks at 15.8–16.8° (2θ) are attributed to the (020) diffraction plane of the monoclinic unit cell with dimensions $a = 5.92$, $b = 10.64$, $c = 6.55$ Å which were previously determined [54]. After a ~250°C post-deposition anneal, α-PPXN begins to transform to β-PPXN which was not complete until successive anneals to 350°C. The peak at 19.70° (2θ) ($a = b = 20.78$ Å) appearing after 250°C and 300°C successive anneals is probably a slightly different (040) hexagonal orientation. However, limited XRD spectra are available for successive post-deposition anneals of PPXN. The other crystal transformations are supposedly reversible, however, the films here is 95 nm. It has been previously shown that the birefringence is strongly affected by the thickness of the PPXN thin film below ~112 nm [44]. The other peak at 20.391° (2θ) in the XRD spectra can be attributed to β-PPXN ($a = b = 20.09$ Å) as reported previously [58].

Correlations between birefringence and crystallinity for PPXN are not easily made since PPXN undergoes the α → β transformation at ~220°C. The transformation is not immediate and therefore a transition regime exists when studying PPXN where at higher temperatures more β-PPXN is formed which markedly increases the percent crystallinity to 82% at a post-deposition anneal temperature of ~380°C, thereafter a rapid decrease in percent crystallinity is evident from Fig. 8 due to the degradation of the polymer film at ~400°C. Apparently transformations such as melting T_m and degradation T_d severely disrupt the ordering of all the parylene polymers studied here, driving the birefringence and crystallization to zero.

The *d*-spacings of PPXN are related to its crystal structure and its local structure. The as-deposited crystal structure of PPXN is the monoclinic alpha form. As with PPXC and VT-4, as-deposited α-PPXN shows a disordered crystal structure becoming more ordered after successive post-deposition anneals to 200°C. After the anneal at 250°C, a driving exists to transform the α crystals to the β crystals. This severely disrupts the α-PPXN *d*-spacing as evidenced by its rapid increase. After the 350°C post-deposition anneal, the α-PPXN totally transformed into β-PPXN. The β-PPXN formed does not decrease in *d*-spacing like α-PPXN due to the nucleation and growth of β-PPXN occurring under more favorable conditions. Any decrease in the FWHM according to Fig. 8 is most primarily due to a crystallite size increase. A rough calculation using the well known Scherrer formula [32] with a Scherrer constant of 1.05 and a FWHM of 0.280 yielded a crystallite size of ~67 nm which is ~71% of the thickness of the thin film. More than likely, the crystallites are not spherical but elongated in the plane of the film due to film thickness (~95 nm). The large crystallite size for the high temperature successive post-deposition anneal of PPXN is not surprisingly since a high percent crystallinity was seen after a ~380°C anneal. At longer annealing times it would be interesting to see how large the crystallites would become and how high the percent crystallinity would become for PPXN. According to Fig. 8, PPXN has the highest percent crystallinity next to VT-4 and then PPXC. This might be expected since PPXN is highly symmetrical. VT-4 should have a high crystallinity due to its high symmetry like PPXN but apparently a larger barrier exists to further crystallization as compared to PPXN. Finally, PPXC exhibited a high percent crystallinity at its maximum ~58%. The disruption of the symmetry of the repeating unit by the introduction of chlorine on the phenyl group would be expected to reduce the crystallinity of PPXC as compared to PPXN. The introduction of chlorine onto PPXN would be similar to the introduction of a methyl group on polyethylene. Even the highly symmetrical isotatic polypropylene exhibits a large reduction in percent crystallinity (62–70%) as compared to high density polyethylene (>90%) [59].

The FWHM (Fig. 10) data for PPXN shows a decrease for β-PPXN most probably due to an increase in crystallite size which causes an increase in percent crystallinity. The change in FWHM of α-PPXN is more complicated. Initially, a slight increase in the FWHM occurs and then a decrease, after which point the α → β transformation occurred. The small increase in FWHM is counter to what was previously seen for PPXC and VT-4. α-PPXN increases in percent crystallinity and its *d*-spacing decreases, therefore, an increase in the FWHM might be indicative as an increase in the stress state of the film, which might be likely and corresponds well to stress studies undertaken on PPXN. A previous study showed the stress state of PPXN to be compressive as-deposited (−18 MPa) and after a 15 min anneal at 200°C the stress state was 40 MPa tensile [37]. Therefore, an increase in the stress state of the thin film is

Table 2
Experimental parameters influencing the separation between adjacent benzene rings

	α-PPXN	VT-4	PPXC/PPXD
van der Waals atomic radii	120 [61] to 145 [62] in pm (H)	150–160 pm [61] (F)	170–190 pm [61] (Cl)
Bond length [60]	109 pm (C–H)	136 pm (C–F)	176 pm (C–Cl)

probable but would not be seen in the FWHM data unless it dominates over the decrease in crystalline disorder and the increase in crystallite size after successive post-deposition anneals.

4. Control of optical anisotropy through repeat unit structure

As previously discussed, the polarizability of the phenyl group is greatest in the plane of the ring. Two adjacent polymer chains (containing a main chain phenyl group) will be most stable if both phenyl groups lie in the same plane due to greater dispersion forces. This type of bonding may also be considered as instantaneous dipole–induced dipole interaction. The energy of such dispersive bonding is [60]:

$$E = -(2\mu\alpha)/r^6 \tag{16}$$

where μ is the mean instantaneous dipole, and α is the atomic or molecular polarizability and r is the separation between adjacent atoms or molecules. Dispersion forces are of extremely short-order and generally weak. Of all the chemical forces or interactions they are generally the weakest. However, they are very important with regards to the bonding of adjacent polymer chains, which is of interest to the present discussion. Much of the energy gained due to specific bonding during polymer crystallization may be associated with the bonding between adjacent polymer chains. Sometimes this is the same chain as in the case of a chain-folded morphology polymer crystallite. These dispersion forces are often weak but two factors make them important and significant: the close association of atoms or molecules ($E \propto 1/r^6$) and the direct proportionality between bond strength and the polarizability of the atoms or molecules. Table 2 shows the atomic radii and bond lengths of the atoms in question which relates to the separation between adjacent phenyl groups (or polymer chains).

Table 3
Lattice spacings of CVD thin film polymers

At $T < 150$°C	α-PPXN	PPXC	PPXD
b-Axis lattice parameter (monoclinic)	10.64 Å	12.77 Å	13.82 Å
At $T \sim 380$°C	β-PPXN	VT-4	
a-Axis lattice parameter (hexagonal)	20.52 Å	21.09 Å	

Table 3 shows direct experimental evidence for the separation between adjacent benzene rings. The *b*-axis lattice parameter from the monoclinic unit cell of α-PPXN, PPXC, and PPXD represents the distance between two phenyl groups (since two repeat units exist per unit cell).

The polarizabilities of hydrogen and fluorine are similar but much larger for chlorine. However, fluorine and chlorine because of their high electronegativties of 4 and 3.45 tend to decrease the polarizability of neighboring atoms or molecules, e.g. phenyl. In the case of chlorobenzene, its overall polarizability is increased to 12.5 $Å^3$ from 10.4 $Å^3$ for benzene due to the high polarizability of chlorine [21]. With the presence of chlorine, the out-of-plane polarizability of chlorine containing benzene increases to 7.58 $Å^3$ for chlorobenzene from 6.65 $Å^3$ for benzene, which will be important in later discussion [63]. The electronic polarizabilities of like molecules containing hydrogen, fluorine, and chlorine are compared in Table 4. This trend found in Table 4 is fairly typical of most molecules which contain a halogen atom, namely fluorination causes a decrease and chlorination causes an increase in electronic polarization relative to the hydrocarbon molecule.

Considering the experimental evidence in Fig. 4 showing PPXN and VT-4 are negatively birefringent (also AF-4) and both PPXC and PPXD are positively birefringent resulting from the relative orientation of the phenyl groups to the substrate apparently the most important parameter affecting this orientation is the separation between adjacent phenyl groups. This is no surprise since the energy of the dispersion forces are proportional to $1/r^6$. However, why does an increase in separation result in orientational differences between hydrogen/fluorine-containing polymers and chlorine containing polymers?

It must be assumed that the crystalline polymer is thermodynamically more stable than an amorphous polymer due to greater specific interactions (in the case here, the dispersion forces between adjacent phenyl groups). Assuming an unstressed state of the polymer thin film and that no other external forces impose on the crystallization or orientation behavior of the thin film polymers studied here, then the relative orientation of the phenyl groups within the

Table 4
Electronic polarizabilities of diatomic molecules/bonds of the form HX and CX

	α-PPXN	VT-4	PPXC/PPXD
α ($Å^3$) [63]	0.819 (H–H)	0.51 (H–F)	2.63 (H–Cl)
α ($Å^3$) [64]	0.65 (C–H)	0.68 (C–F)	2.61 (C–Cl)

crystallized phase of the polymer thin film is also the most stable orientation. A compromise then exists between 100% positive birefringent orientation where little molecular polarizability exists to stabilize adjacent phenyl bonding and 100% negative birefringent orientation which is destabilized due to the presence of chlorine. Further, the presence of chlorine results in a greater out-of-plane polarizability for the benzene ring (7.58 $Å^3$ for chlorobenzene 6.65 $Å^3$ for phenyl) thus stabilizing the rotated phenyl groups [64]. Based on the difference in bond lengths between C–H and C–Cl, the distance between adjacent phenyl groups for PPXC (as opposed to α-PPXN) should increase by 61%. Based on the difference in van der Waals atomic radii between atomic hydrogen and atomic chlorine this distance should increase by 38%. However, when the *b*-axis of the monoclinic unit cell is experimentally measured for PPXC it increased only 20% over α-PPXN. The rotation of the benzene rings then allows a closer association between adjacent benzene rings thus creating stronger interactions. Since the bond strength of dispersion forces between molecules is proportional to $1/r^6$ then a difference of a few angströms results in much larger differences in bond stability.

A simple example to help illustrate this point is: a 50% increase in the *b*-axis for PPXC to 15.96 Å (assuming no rotation for the phenyl groups and no increase in polarizability) would decrease the bond strength 11 times. With the rotation of the phenyl groups, the *b*-axis only increases by 20% to 12.77 Å thus decreasing the PPXC bond strength relative to α-PPXN 3 times. Moreover, an increase in the out-of-plane polarizability for the chlorine-containing phenyl group occurs due to the chlorine's high isotropic polarizability. This increase in polarizability increases the bond stability of the rotated benzene rings. However, the more significant parameter affecting bond strength is the distance between adjacent molecules since the polarizability is directly proportional to bond strength and distance is related by $1/r^6$. The *b*-axis length for PPXD only increased 8% over that of PPXC according to Table 2. In addition, a second chlorine atom should increase the out-of-plane polarizability of the chlorine containing phenyl group to a greater extent. Therefore, it should be expected that PPXD's crystallites are more stable than those of PPXC. A means to test this stability is indirectly through the melting points of the parylene polymers.

The weaker interaction between adjacent phenyl groups due to an increase in intermolecular distance is also reflective in the melting points of the polymer thin films. However, one complication exists, namely the rotational inertia of the phenyl group also significantly affects the polymer's melting temperature. The trend is still obvious PPXN (420°C), VT-4 (402°C), PPXC (293°C), and PPXD (380°C). The rather large increase from 293°C to 380°C for PPXC and PPXD is reflective in an increase in bond stability due to the increase in the out-of-plane polarizability of the chlorine-containing phenyl group and to a lesser extent an increase in rotational inertia of PPXD's phenyl group.

5. Conclusions

The increasing demand for low dielectric constant ($k < 3.0$) CVD polymer thin films to replace SiO_2 to reduce *RC*-delay in ULSI devices has prompted the synthesis of many new polymers. The ultimate properties of the polymer thin films are determined by their anisotropy or local bonding. That anisotropy for polymer thin films is complex and is strongly affected by the thermal history of the polymer. A strong understanding of the structure–property relations and how they are influenced by the molecular architecture is imperative for the future development of polymer thin films.

The study here has shown the value of birefringence measurements as a function of successive post-deposition anneals. Birefringence is sensitive to the relative orientation of the phenyl group which is influenced by physical transformations such as crystallization, melting and film degradation. Correlations between birefringence measurement were made with X-ray diffraction measurements primarily in terms of the crystallization of the thin films. XRD data had shown a large degree of crystal disorder for VT-4, the presence of stress in the α form of PPXN and other conclusions dealing with the anisotropic changes in all of the polymer thin films studied here.

References

[1] Lee WW, Ho PS. MRS Bull 1997;22:19–23.
[2] Pan C, Ali T, Ling Y, Chiang C. Polym Prepr 1996;37:152–3.
[3] Hu HSW, Griffith JR, Buckley LJ, Snow AW. ACS Symp Ser: Microelect Tech. Ser 1995;614:369–78.
[4] Lee YK, Murarka SP, Jeng SP, Auman B. Mat Res Soc Symp Proc 1995;381:31–43.
[5] Auman B. Mat Res Soc Symp Proc 1995;381:19–29.
[6] Lu TM, Moore JA. MRS Bull 1997;22:28–31.
[7] Gaynor JF, Senkevich JJ, Desu SB. J Mater Res 1996;11:1842–50.
[8] You L, Yang GR, Lang CI, Moore JA, Wu P, McDonanld JF, Lu TM. J Vac Sci Tech A 1993;11:3047–52.
[9] Treloar LRG. Trans Faraday Soc 1940;36:538.
[10] Smith KJ, Puett DJ. J Appl Phys 1966;37:346–54.
[11] Mark JE, Llorente MA. Polym J 1981;13:543–53.
[12] Stein RS. Chem Rubber Tech 1976;49:458.
[13] Llorente MA, Mark JE. J Polym Sci, Polym Phys Ed 1981;19:1107–20.
[14] Anaka Y, Stein RS. J Polym Sci, Polym Phys Ed 1975;13:2195–219.
[15] Matsuo M, Ooki J, Harashina Y, Ogita T, Manley RStJ. Macromolecules 1995;28:4951–60.
[16] Treloar LRG. Trans Faraday Soc 1947;43:284–93.
[17] Flory PJ. J Chem Phys 1947;15:379.
[18] Stein RS. Polym Prepr 1975;16:387.
[19] Stein RS. Polym Engng Sci 1976;16:152.
[20] Su TK, Stein RS. Bull Am Phys Soc Ser II 1975;20:340.
[21] Dewar MJS, Stewart JJP. Chem Phys Lett 1984;111:416–20.
[22] Stein RS, Winter HH, Müller J, Srinivasarao M. Pure Appl. Chem. 1995;67:1971–82.
[23] Hasegawa T, Umemura J, Takenaka T. J Phys Chem 1993;97:9010–2.

[24] Hasegawa T, Takeda S, Kawaguchi A, Umemura J. Langmuir 1995;11:1236–43.
[25] Sakamoto K, Arafune R, Ito N, Ushioda S, Suzuki Y, Morokawa S. Jpn J Appl Phys 1994;33/2(9B):L1323–6.
[26] Nobbs JH, Bower DI, Ward IMJ. Polym Sci, Polym Phys Ed 1979;17:259.
[27] Osaki S, Tashiro K. Macromolecules 1998;31:1661–4.
[28] Osaki S. Polym J 1987;19:821–8.
[29] Pazur RJ, Prud'homme RE. J Polym Sci: Polym Phys 1994;32:1475–84.
[30] Wilchinsky ZW. J Appl Phys 1960;31:1969.
[31] Wilchinsky ZW. Advances in X-ray analysis, 6. New York: Plenum Press, 1963 p. 231.
[32] Alexander LE. X-ray diffraction methods in polymer science, New York: Wiley, 1969 pp. 198–279.
[33] Stein RS. J Polym Sci 1958;31:327.
[34] Wilchinsky ZW. J Appl Phys 1959;30:792.
[35] Wilkes GL. Encyclopedia of polymer science and engineering, 14. New York: Wiley, 1989 pp. 542–621.
[36] Cammarata RC, Bilello JC, Greer AL, Sieradzki K, Yalisove SM. MRS Bull 1999;24:34–38.
[37] Dabral S, Etten JE, Apblett C, Yang GR, Ficalora P, McDonald JF. Mat Res Soc Symp Proc 1992;239:113–7.
[38] Fukuda M, Wilkes GL, Stein RS. J Polym Sci Part 2-A 1971;9:1417–47.
[39] Stein RS, Hong SD. J Macromol Sci Phys 1976;12:125–51.
[40] You L, Yang GR, Knorr DB, McDonald JF, Lu TM. Appl Phys Lett 1994;64:2812–4.
[41] Isoda S, Tsuji M, Ohara M, Kawaguchi A, Katayama K. Polymer 1983;24:1155–6147.
[42] Stein RS. Rub Chem Tech 1976;49:458–535.
[43] Morgan RJ, Treloar LRG. J Polym Sci Part 2-A 1972;10:51.
[44] Senkevich JJ, Desu SB. Mat Res Soc Symp Proc 1998;511:139–44.
[45] Kirkpatrick DE, Wunderlich B. Makomol Chem 1985;186:2595–607.
[46] Ryan ET, McKerrow AJ, Leu J, Ho PS. MRS Bull 1997;22:49–54.
[47] Gurnee EF, Patterson LT, Andrews RD. J Appl Phys 1955;26:1106–10.
[48] Isoda S, Kawaguchi A, Katayama K-I. J Polym Sci: Polym Phys Ed 1984;22:669–79.
[49] Eisele R. Introduction to polymer physics, Berlin: Springer, 1990. pp. 92–3.
[50] Marand H, Xu J, Srinivas S. Macromolecules 1998;31:8219–29.
[51] Kakudo M, Kasai N. X-ray diffraction by polymers, Amsterdam: Elsevier, 1972 pp. 111–33.
[52] Wunderlich B. Angew Chem (Int ed) 1968;7:912–9.
[53] Kubo S, Wunderlich B. J Appl Phys 1971;42:4558–65.
[54] Kubo S, Wunderlich B. J Appl Phys 1971;42:4565–70.
[55] Kubo S, Wunderlich B. J Polym Sci: Polym Phys Ed 1972;10:1949–66.
[56] Treiber G, Boehlke K, Weitz A, Wunderlich B. J Polym Sci: Polym Phys Ed 1973;11:1111–6.
[57] Niegisch WD. J Appl Phys 1966;37:4041–5.
[58] Surendran G, Gazicki M, James WJ, Yasuda H. J Polym Sci, Part A: Polym Chem 1987;25:1481–503.
[59] Brandrup J, Immergut EH, editors. Polymer handbook 3. New York: Wiley, 1989.
[60] Huheey JE. Inorganic chemistry: principles of structure and reactivity, New York: Harper Collins, 1983.
[61] Bondi A. J Phys Chem 1968;68:441.
[62] Allinger NL, et al. J Am Chem Soc 1968;90:1199.
[63] Bottcher HCP, Bottcher CJF, Borkewijk P. Theory of electric polarization, Amsterdam: Elsevier, 1978.
[64] Denbigh KG. Trans Faraday Soc 1940;36:936–48.